Numerical modelling of erosion processes in the Himalayas of Nepal: effects of spatial variations of rock strength and precipitation

V. GODARD[1], J. LAVÉ[2] & R. CATTIN[1]

[1]*Laboratoire de Géologie, Ecole Normale Supérieure, 24, rue Lhomond, 75005 Paris, France (e-mail: godard@geologie.ens.fr)*

[2]*Laboratoire de Géodynamique des Chaînes Alpines, CNRS, 1381, rue de la Piscine, 38400 St-Martin d'Hères, France*

Abstract: The interplay between tectonics and erosion has a predominant control on the evolution of the morphology of mountain belts. Here we investigate the modalities of deformation in Central Nepal on a *c*. 100 ka time scale in response to tectonic and external forcings, through the use of a finite-element thermomechanical model coupled with an integrative denudation formulation that accounts for fluvial incision and hillslope landsliding. We study the complex coupling existing between tectonics and erosion, with special emphasis on the influences of rock strength and rainfall distributions. Our results underline the key role played by lithologic variations in the elevation of both rivers and mean topography. We show that the location of the Main Frontal Thrust is mainly controlled by the low erodability of the unconsolidated sandstone in the Siwaliks Hills. As previously suspected (Burbank *et al.* 2003), our simulations demonstrate that the pattern of uplift in Nepal is mainly dependent on both erodability and fault geometry, rather than on rainfall distribution.

It has long been understood that the landscape of mountain belts is the result of the balance between tectonic uplift and surface processes, as modulated by denudation and sedimentation (Molnar 2003). Outside glaciated regions, river incision into bedrock has been recognized as a primary agent in both landscape evolution and large-scale surface mass transport (e.g., Burbank *et al.* 1996; Willett 1999; Whipple & Tucker 1999; Lavé & Avouac 2001). Erosion influences tectonics by modifying the mass distribution in the orogen, which controls the isostatic response and the strain localization. On the other hand, tectonic uplift or subsidence is related to the distribution of erosion and sedimentation zones.

Over the last fifteen years many numerical models have been developed to study feedbacks and interactions between tectonics and denudation in mountainous areas. However, in most of these models, transport of mass at the surface is either reduced to a diffusion law (Avouac & Burov 1996; Cattin & Avouac 2000), to a linear function of the local slope (Beaumont *et al.* 2001), or to a simple fluvial incision law where the mean topographic profile is represented by a river profile (Willett 1999). Those approaches do not take into account the dual nature of denudation in mountain ranges, which combines river bedrock incision and hillslope landsliding.

Here we explore how patterns of precipitation and rock strength affect both river and topographic profiles across the range of the Himalayas and southern Tibet. Following the approach of Godard *et al.* (2004) we have coupled a 2D thermomechanical model, which includes localization of deformation through frictional faults, to a surface process model based on a detachment-limited fluvial incision law. In contrast with Willett (1999), the mean topographic profile is computed using both the calculated trans-Himalayan river profile and an implicit description of the tributaries and hillslopes (Lavé 2005). Our purpose here is to evaluate the importance of rainfall and rock strength distributions in controlling the modalities of landscape denudation. We investigate the response of the mechanical model to forcings corresponding to variations of those two parameters. We first review the geodynamic and hydrological setting of the study area that encompasses the Himalayas of Nepal from the Gangetic Plain to the southern edge of the Tibetan Plateau. Next, we describe the modelling approach and the surface processes formulation introduced as a boundary condition at the surface of the model. Then, we present the behaviour of a reference

From: BUITER, S. J. H. & SCHREURS, G. (eds) 2006. *Analogue and Numerical Modelling of Crustal-Scale Processes.* Geological Society, London, Special Publications, **253**, 341–358.
0305-8719/06/$15.00

model which closely mimics the main features of the Himalayan–Tibetan system. Starting from this reference model, the sensitivity of the results to rock strength and rainfall distribution is investigated.

Geodynamical setting

Himalayan tectonics

The Himalaya results from the collision between India and the southern edge of Eurasia. Since *c.* 20 Ma, tectonic and erosive processes have built an impressive landscape characterized by a steep topographic front from the 5000 m elevation Tibetan Plateau down to the Gangetic plain. Four major morphotectonic domains are usually recognized from north to south: the low-relief South Tibetan plateau, the High Himalaya (HH) with deep gorges and *c.* 8000 m summits, the mountainous to hilly relief of the Lesser Himalaya (LH), and the frontal low elevation relief of the Siwalik Hills (Fig. 1). The Himalayan range results from the successive activation of major thrust zones: the main central thrust (MCT) and the main boundary thrust (MBT) (Le Fort 1986). These two faults are presumed to branch upward from a major mid-crustal décollement, the main Himalayan thrust (MHT) (Schelling & Arita 1991; Zhao *et al.* 1993; Pandey *et al.* 1995; Lavé & Avouac 2001). Coeval with thrusting, the Indo-Gangetic foredeep formed in front of the rising Himalaya and accumulated several kilometres of Cenozoic molasse deposits, material eroded from the areas of high relief. Thin-skinned thrust-faulting has incorporated these sediments into the hanging walls of several thrusts, now expressed as the Siwaliks Hills. These frontal faults branch from the MHT, which roots at a depth of 30–40 km beneath the South Tibet (Zhao *et al.* 1993), and displays a ramp-and-flat geometry beneath the HH and LH domains (Schelling & Arita 1991; Pandey *et al.* 1995; Lavé & Avouac 2001). The long-term shortening rate across the range is *c.* 20 mm yr^{-1} (Lyon Caen & Molnar 1985; Armijo *et al.* 1986) and is similar to present convergence imaged by GPS (Bilham *et al.* 1997). In central Nepal, geomorphic evidence

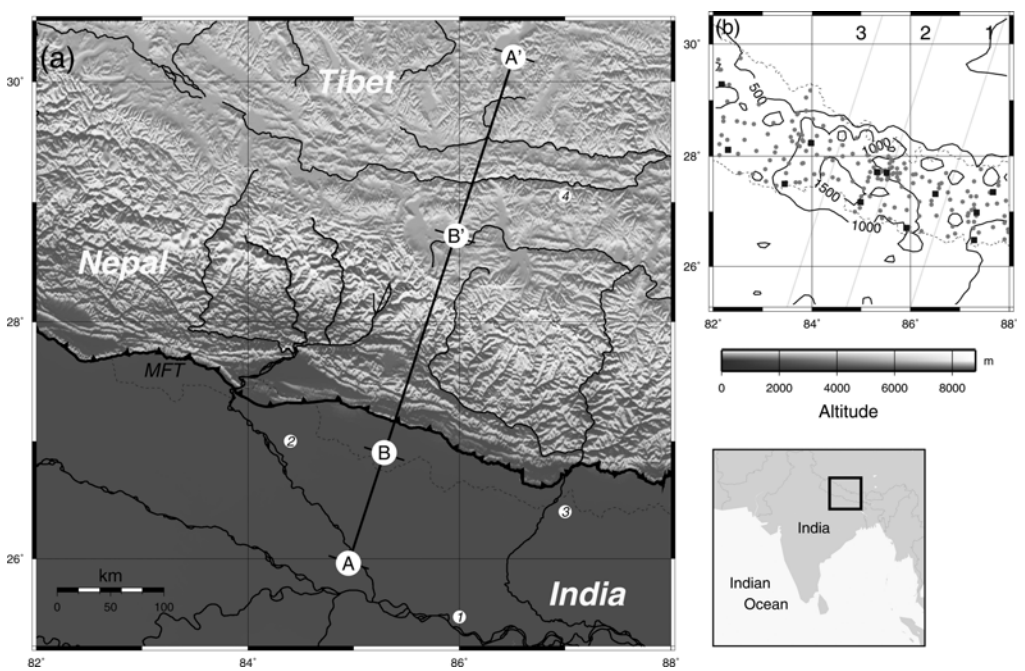

Fig. 1. Situation. (**a**) Topographic map of the study region (GTOPO30 DEM), showing the principal hydrographic features, the position of the main frontal thrust, and the cross sections AA′ (Fig. 3) used in the modelling and BB′ presented on Fig. 8. 1 – Ganga, 2 – Narayani, 3 – Sapt Kosi, 4 – Tsangpo. (**b**) Rainfall map derived from NOAA (2005) estimates. The position of the 3 cross-sections of Fig. 2 is indicated. Light grey dots and dark grey squares represent the rain gauges of GAME (2005) and NMFD (2005) networks, respectively.

suggests in addition that most of the present shortening across the Himalayas is transferred toward the main frontal thrust (MFT) (Lavé & Avouac 2000).

Precipitation, hydrology and erosive processes

Precipitation in Nepal is mainly controlled by the barrier of the Himalayas, with a brutal condensation against the HH of the wet air coming from the Indian Ocean during the monsoon. Whereas a marked rain shadow develops on the northern flank of the HH, the prominent fluvial network of the southern flank, fed by intense rainfall, is deeply entrenched in the topography and actively contributes to the denudation of the orogen. Important lateral variations of the distribution of rainfall exist in Nepal (Figs 1 and 2), but, despite the amplitude of change, the consistent main patterns are the increasing precipitation from the Gangetic plain to the HH, the orographic barrier of the HH, and the low precipitation on the Tibetan Plateau. Several major north-south rivers drain the Himalayas of Nepal from southern Tibet down to the Indo-Gangetic plain. In Central and East Nepal, across the HH, those trans-Himalayan rivers are on average *c*. 50 km apart before joining, in the southern part of the LH, two major rivers systems, the Narayani and

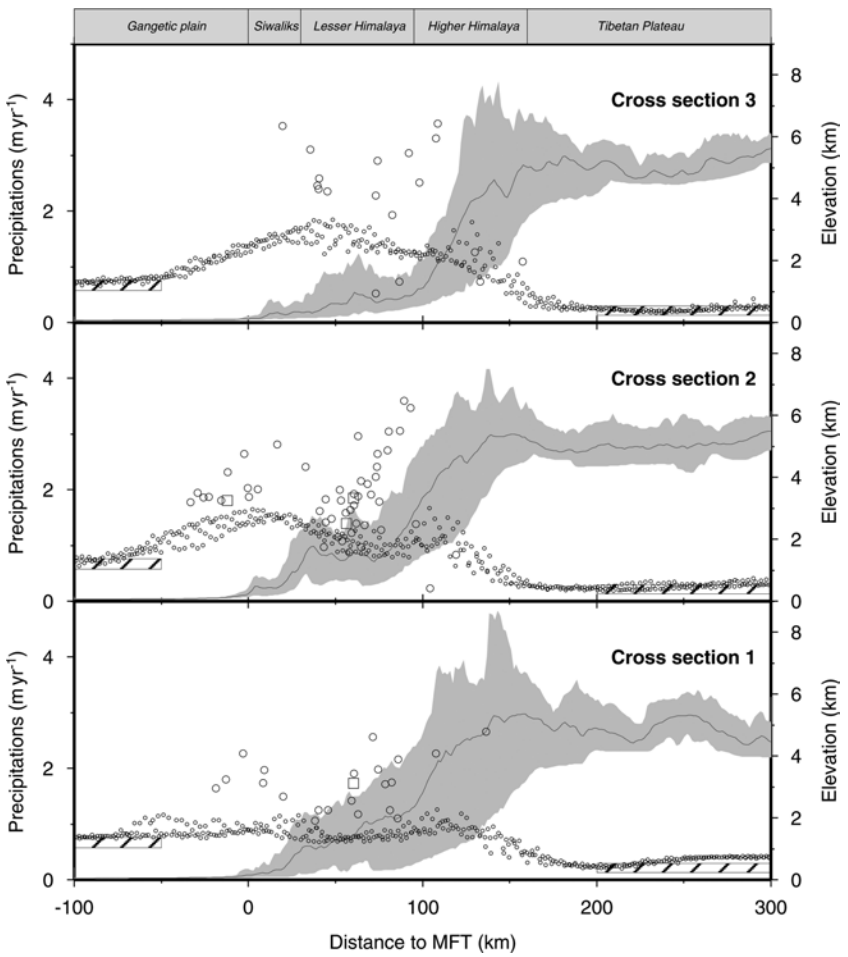

Fig. 2. Projection of the precipitation data on the three swathe profiles presented in Fig. 1, with corresponding mean elevation from GTOPO30 DEM (grey area indicates minimal and maximal values). Dots derive from NOAA dataset and circles and squares refers to measurements from GAME (2005) and NMFD (2005) gauge networks, respectively. Dashed boxes in Tibet and India represent compilation of data from GAME (2005) and IITM (2005), respectively. All swathes are 100 km wide.

Sapt Kosi basins. Both rivers are tributaries of the Ganga (Fig. 1). Trans-Himalayan rivers and fluvial terraces profiles in Nepal (Lavé & Avouac 2000, 2001), and cosmogenic data in India (Vance *et al.* 2003) suggest that erosion is maximal across the Siwaliks and the HH, lower in the LH, and minimal in South Tibet.

Modelling approach

Geometry of the system

Our model is based on a 700 km long N18°E cross-section perpendicular to the range, from the Gangetic Plain to the Tibetan Plateau (see Fig. 1 for the location). The principal geometric characteristics of our model are similar to Cattin and Avouac's model (2000) and our previous work (Godard *et al.* 2004) and are presented in Figure 3. The geometry of the Moho beneath South Tibet is derived from INDEPTH seismic profile (Zhao *et al.* 1993) and from gravity data (Cattin *et al.* 2001). The initial elevation for both river and mean topography mimics the main features of the present day topography.

Rheology

We use a 2D Lagrangian finite element code (Hassani *et al.* 1997) that allows us to solve the constitutive rheological equations expressing the relationships between stress and strain tensors ($\underline{\underline{\sigma}}$ and $\underline{\underline{\varepsilon}}$, respectively). The behaviour of the materials is considered elasto-visco-plastic. The elasticity is expressed by Hooke's law (see specification of parameters in Table 1),

$$\varepsilon_{ij} = \frac{1+\nu}{E}\sigma_{ij} - \frac{\nu}{E}\mathrm{trace}(\underline{\underline{\sigma}})\delta_{ij} \qquad (1)$$

while the non-Newtonian viscous behaviour, dependent on temperature T, is controlled by the following relationship between deviatoric stress and strain rate $\dot{\varepsilon}$,

$$\dot{\varepsilon} = \gamma_0(\sigma_1 - \sigma_3)^n e^{E_a/RT} \qquad (2)$$

where σ_1 and σ_3 are the maximum and minimum principal stresses, respectively. The limit between the visco-elastic and the plastic domains is defined by a Drucker-Prager failure

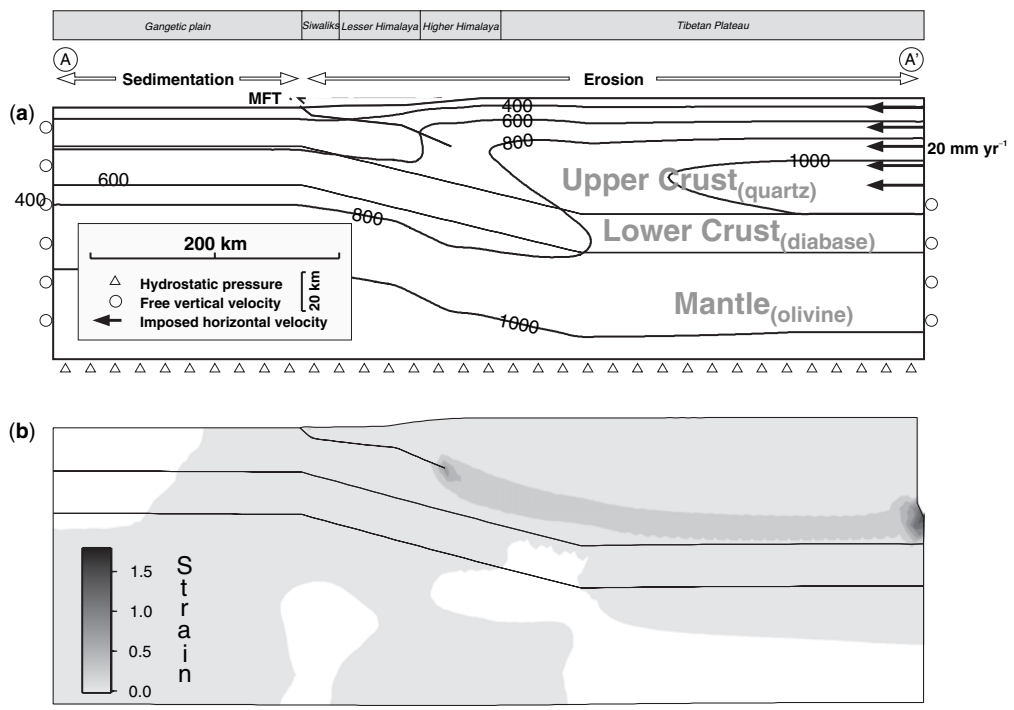

Fig. 3. Main features of the model. (**a**) Geometry of the system, temperature field (K), rheological units, and boundary conditions used for the modelling. In the foreland sedimentation balances subsidence. In the range, landscape evolution is controlled by the fluvial incision law. (**b**) Second invariant of the deviatoric strain tensor at the end of the simulation. Horizontal and vertical dimensions of model are 700 km and 130 km, respectively.

Table 1. *Rheological parameters used for the mechanical model*

	Quartzite	Diabase	Olivine
Density, ρ (kg m^{-3})	2900	2900	3300
Young modulus, E (Gpa)	20	20	70
Poisson's ratio, ν	0.25	0.25	0.25
Cohesion, c (Mpa)	10	10	10
Internal friction angle, ϕ	30°	30°	30°
Standard fluidity, γ_0 (Pa^{-n} s^{-1})	6.03×10^{-24}	6.31×10^{-20}	7.00×10^{-14}
Power law exponent, n	2.72	3.05	3.0
Activation energy, E_a (kJ mol^{-1})	134	276	510

Parameters from Carter & Tsenn 1987; Tsenn & Carter 1987; Kirby & Kronenberg 1987. Universal gas constant $R = 8.314$ J mol^{-1} K^{-1}.

criterion, according to,

$$\frac{1}{2}(\sigma_1 - \sigma_3) = \left(c(\cot\phi) + \frac{1}{2}(\sigma_1 + \sigma_3)\right) \times \sin\phi \quad (3)$$

Godard *et al.* (2004) have shown that a composite quartz-diabase rheology associated with a fluvial incision law is required to explain both erosion rate and topographic profile in the Himalayas. Three layers are distinguished for the lithosphere: the upper and lower crusts, and the upper mantle. Each layer has specific mechanical properties. We use the empirical rheological equations and laboratory-derived material properties for quartz, diabase and dry olivine (Table 1). The temperature field from Henry *et al*. (1997) (Fig. 3) is used to compute the viscosity of the material. Considering the typical duration (*c.* 100 ka) of our simulations, we do not solve the heat equation. This temperature field is thus considered stable, relative to the mesh, over the run.

Boundary conditions

The boundary conditions applied to the system are constrained by geodynamical data. Most of the observations available in this area (see Fig. 8 caption), including GPS measurements (Bilham *et al.* 1997; Larson *et al.* 1999) estimate a shortening rate of 20 mm yr^{-1}. Recently, Chen *et al.* (2004) suggested velocities closer to 13 mm yr^{-1}. A variation of this magnitude in convergence rate does not modify significantly our conclusions. We apply, therefore, a 20 mm yr^{-1} horizontal velocity on the northern vertical face to a depth of 40 km, which is the depth of the high temperature and low viscosity zone under Tibet, used as a decoupling level in the crust. Vertical velocities on the other vertical faces are left free. The structure is supported by hydrostatic pressure at its base, which allows isostatic compensation and thus generates a coupling between rock-uplift and denudation.

A fault with a simple Coulomb friction law is introduced and follows the ramp-and-flat geometry proposed for the MHT. Due to the duration of our simulations we consider long-term deformation, which integrates a large number of seismic cycles, and slip on a low friction MHT ($\mu = 0.01$) is considered as continuous (Cattin & Avouac 2000). This low frictional surface connects to a mid-crustal high temperature zone that allows the localization of a narrow ductile deformation zone corresponding to the continuation of the MHT (Fig. 3), imaged by the INDEPTH experiment (Zhao *et al.* 1993).

The main purpose of this study is to focus on the influence of the surface processes applied to the topography as a boundary condition. We distinguish two domains in term of surface processes: the foreland south of the MFT ($x < 0$), with active sedimentation, and the mountain range north of the MFT, dominated by active erosional processes. The first domain, the Indo-Gangetic basin is classically described as a low elevation over-filled basin (Lyon-Caen & Molnar 1985): we thus assume in the following a constant *c.* 0 m elevation for it. The characteristics of the fluvial incision formulation used in the range are described further down.

Numerical method

The approach used here for simulating tectonic processes employs the dynamic relaxation method (Underwood 1983) coupled with the finite element method. The dynamic relaxation (DR) method is an explicit iterative method for the static solution of mechanical problems. The method can easily take into account large deformations of materials with non-linear behaviour. It is based on the fact that the static solution is the steady-state part of the transient response

for a temporal load,

$$M\ddot{q} + C\dot{q} + Kq = F_e \tag{4}$$

with q, $\dot{q}$ and $\ddot{q}$ the displacement, velocity and acceleration vectors, respectively. C is the damping matrix, K the stiffness matrix, and F_e the external forces applied on the system, respectively. M is the fictitious mass matrix, which can be chosen to be non-singular. The DR algorithm evaluates in each time step the unbalanced forces, that is, the acceleration $\ddot{q}$ due to the disequilibrium between external and internal forces,

$$\ddot{q} = M^{-1}(-C\dot{q} - Kq + F_e) \tag{5}$$

The quantity $C\dot{q}$ represents a numerical viscosity introduced for stabilization purposes, and Kq is the internal forces computed from the integration of the constitutive material laws (Eqns 1, 2 and 3).

The time integration scheme computes velocity and displacement using an explicit (forward in time) finite difference method. The explicit algorithm is conditionally stable, the condition being

$$\Delta t \leq \frac{2}{\omega_{\max}} \tag{6}$$

where $\lambda_{\max} = \omega_{\max}^2$ is the highest eigenvalue of the matrix $M^{-1}K$.

Time scenario and stability

The total duration of the simulations is *c.* 320 ka, with an effective simulation duration (Fig. 4) of 80 ka and a time step of 1.5 yr. The elements are triangular with a typical size (diameter of circumscribing circle) of 3 km.

The convergence of the algorithm is associated with the minimization of unbalanced forces (i.e., acceleration); the different processes acting on the system are thus introduced gradually (Fig. 4). The simulation is divided into two steps: (1) a stabilization period where tectonics and denudation are introduced

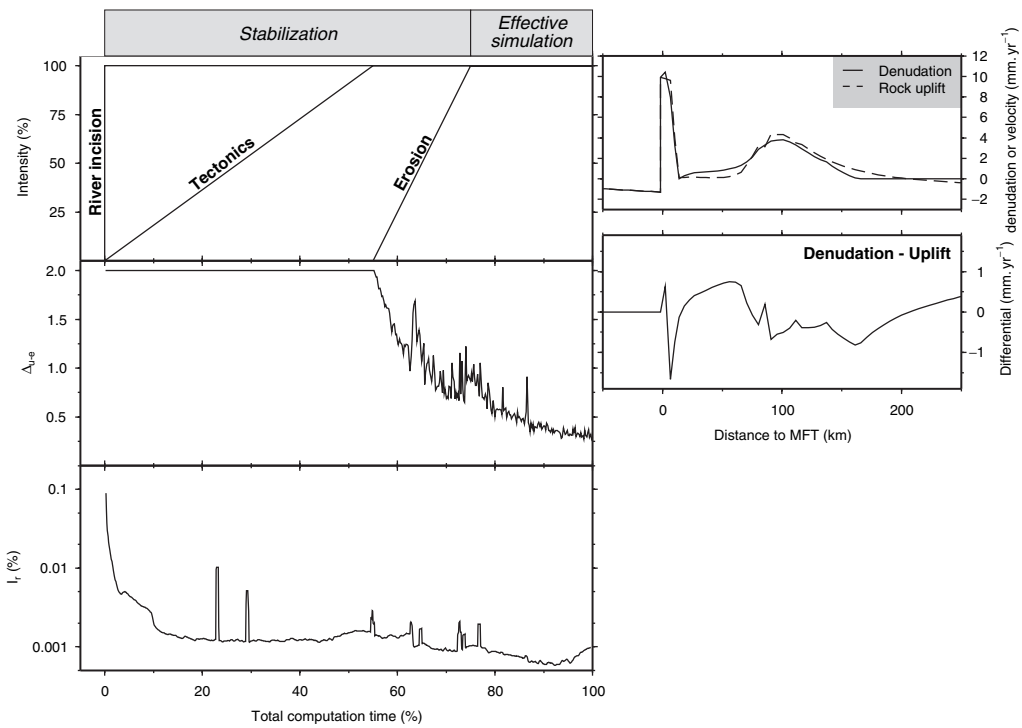

Fig. 4. Time scenario of boundary conditions (see Fig. 6 for details on the relationship between the tectonic computation and the surface processes), evolutions of the inertial ratio (I_r, Eqn 7) and of the difference between uplift and denudation (Δ_{u-e}, Eqn 8). See text for details. The uplift and denudation profiles at the end of the computation, and their difference, are also plotted.

progressively, (2) an effective simulation period, when all the processes act at full intensity. The initial river profile is the same as the initial mean topographic profile. Starting fluvial incision before topographic denudation is thus necessary to promote the stabilization of the river (i.e., convergence toward the steady-state profile) and to allow a significant entrenchment to exist at the beginning of the effective simulation period, thereby initiating topographic denudation. To evaluate the stability of the computation, we use the inertial ratio, I_r computed as,

$$I_r = \frac{\left\|\vec{F_e} + \vec{F_i} + \vec{F_c}\right\|}{\left\|\vec{F_e}\right\| + \left\|\vec{F_i}\right\| + \left\|\vec{F_c}\right\|} \tag{7}$$

where $\|\vec{F_e}\|$, $\|\vec{F_i}\|$ and $\|\vec{F_c}\|$ are respectively the external, internal and reaction forces acting on the system. The mechanical steady state is defined as an average equilibrium between uplift and denudation rates, which is computed as the average, at each point along the profile, of the normalized difference between denudation, e_i, and rock-uplift, u_i,

$$\Delta_{u-e} = \frac{\sum_{i=1}^{N_p} |u_i - e_i|}{\sum_{i=1}^{N_p} (u_i + e_i)/2} \tag{8}$$

The time limit of the simulations is imposed by distortions of the mesh in high erosion areas (Siwaliks foothills).

Figure 4 shows that the inertial ratio I_r is lower than 0.01% during the effective simulation period, which attests to the overall numerical stability of the model. The slight increase of the ratio at the end of the run is associated with the reduction of the size of the elements due to erosive processes. During the effective simulation period, Δ_{u-e} converges toward a constant value of *c.* 0.3 which indicates a slight degree of disequilibrium. Part of the mismatch between uplift and erosion corresponds to the contribution of horizontal velocity to uplift. Our main concern is to reach a relative equilibrium that allows inter-model comparison.

Surface processes

Fluvial incision

Recent studies have underlined the key role played by fluvial incision in driving unglaciated landscape denudation (Whipple & Tucker 1999). Whereas different functional forms have been proposed to model fluvial incision (Whipple & Tucker 2002), in an attempt to develop a simple approach, we have used a detachment-limited relation that provides satisfying first-order results in the Subhimalaya (Lavé & Avouac 2001). This approach states that the bedrock incision rate of a river, at abscissa x, is proportional to the fluvial shear stress τ_x in excess of some threshold τ_c:

$$\left(\frac{\partial h_{\text{riv}}}{\partial t}\right)_x = K_x(\tau_x - \tau_c) \tag{9}$$

with $\tau_x = \rho \cdot g \cdot H_x \cdot S_x$, ρ the density of water, S_x the river slope, H_x the flow depth and K_x an erodability coefficient that primarily depends on rock strength with respect to abrasion (Lavé & Avouac 2001), but which could mask hidden dependencies on sediment flux and flood distribution. For the sake of simplicity, we will ignore the two latter variables. The shear stress τ represents the force exerted by the flowing water on an area unit of the channel bottom, and is derived from energy expenditure equation. Assuming Manning's equation to describe mean water flow velocity, and employing a scaling law between river width and discharge, it can be shown (Howard *et al.* 1994) that shear stress can reduce to an expression of channel slope and drainage area. The central Himalaya, like many other mountain ranges, displays a relative cylindrical structure and linear drainage systems perpendicular to the range axis. Along these linear drainage systems, 50 km apart, the drainage area is linearly related to the cross-range distance (Fig. 5). Shear stress can then be expressed by:

$$\tau_x = k_1(\bar{P}_x - P_r)^{\gamma}(L(X - x))^{\beta}\left(\frac{S_x}{s_0}\right)^{\alpha} \tag{10}$$

where k_1 is a coefficient that depends on the river network geometry and sediment size, L the width of the watershed, s_0 the average sinuosity of the main stream (Fig. 5) and α, β, γ are constant exponents. $\overline{P}$ is the average precipitation on the watershed and P_r some threshold runoff. X is the abscissa of the drainage divide. The values of these parameters are given in Table 2.

Landscape denudation by fluvial incision and landslides

Many numerical models (e.g., Willett 1999) compute the denudation rates applied to topography directly from Equation 9. However, despite their prominent role, the main rivers do not account for the mean topography, which is the pertinent variable for the upper boundary

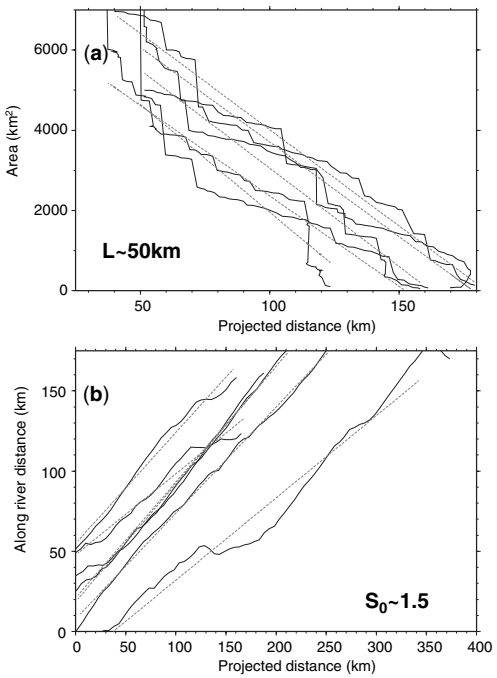

Fig. 5. Two examples of parameter determination for the fluvial incision formalism. (**a**) Evolution of the area of the watershed of some major Trans-Himalayan rivers as a function of projected distance (abscissa on a N18° trending line) illustrating the existence of a linear relationship between those two parameters. The slope of the fit (dashed line) gives the width L of the watershed, ranging from 45 to 53 km. (**b**) Evaluation of the sinuosity for some major Trans-Himalayan rivers through the relation between projected distance (N18°) and along river distance (measured along the river path). The slope of the fit (dashed line) gives the inverse of sinuosity $1/s_0$, sinuosity ranges from 1.4 to 1.9. Fluvial network and watersheds extracted from a 90 m DEM.

Table 2. *Denudation law parameters*

Parameter	Value
Hillslope angle of repose, θ_c (degrees)	40
Himalayan valley width, L (km)	50
Sinuosity, s_0	1.5
Slope exponent, α	0.7
Area exponent, β	0.27
Precipitation exponent, γ	0.33
Critical shear stress, τ_c (Pa)	30
k_1 (Pa m$^{-0.87}$ s$^{0.33}$)	5677
k_2 (Pa m$^{-1.03}$ s$^{0.33}$)	2400
Threshold runoff, P_r (m)	0.2

From Lavé & Avouac (2001) or Himalayan river measurements (e.g., Fig. 5).

condition of mechanical modelling. The elevation profile of the trans-Himalayan rivers in fact represents the base level for the network of tributaries that are draining the whole topography, from their sources at the base of the hillslopes to their confluence with the trunk stream. At a given abscissa, the mean elevation of the topography $\bar{h}$ is therefore the sum of three contributions: (1) the elevation of the main river h_{riv}, (2) the fluvial relief associated to the tributaries Δh_{trib} that we assume to be controlled by the same incision law as the main river, and (3) the mean relief of the hillslope from the fluvial network to the crest, Δh_{hill}. In active orogens, hillslopes are dominated by landslides (Hovius *et al.* 1997); we thus assume that they display a critical slope angle of repose θ_c and that they react instantaneously to any local base-level drop. A new formulation to integrate the fluvial relief associated with the tributary network (Lavé 2005) enables computation at each time step of the changes of the elevation of the trunk stream from Equation 10 and the changes in mean topography according to

$$\left(\frac{\partial \bar{h}}{\partial t}\right)_x = \left(\frac{\partial h_{\text{riv}}}{\partial t}\right)_x + K_x(k_2(P_x - P_r)^{\gamma} \times \Delta h_{\text{trib}_x}^{\alpha} - \tau_c) \tag{11}$$

with,

$$\Delta h_{\text{trib}} = \Delta h_{\text{total}} - \Delta h_{\text{hill}} = \Delta h_{\text{total}} - \frac{\Delta l}{2}\tan\theta_c \tag{12}$$

where k_2 is a coefficient which depends on the tributary network geometry and Δl is the horizontal distance between the crest and the base of the hillslope.

The solving scheme is based on the interplay between two profiles: the mean elevation profile and the river profile (Fig. 6). The river profile is advected with the tectonic velocity field computed by the mechanical solver and the incision rates computed from Equation 10. The mean topographic profile constitutes the upper boundary of the mechanical model. Feedback between tectonics and erosion is achieved by this dynamic interface: (1) the mean topography is advected with the tectonic velocity field and the denudation rates from Equation 11, and (2) the internal stress field is affected by mass removal from the mean topography by denudation processes.

The above formulation does not satisfy, strictly speaking, the mass conservation equation and could be viewed as incomplete. However, in

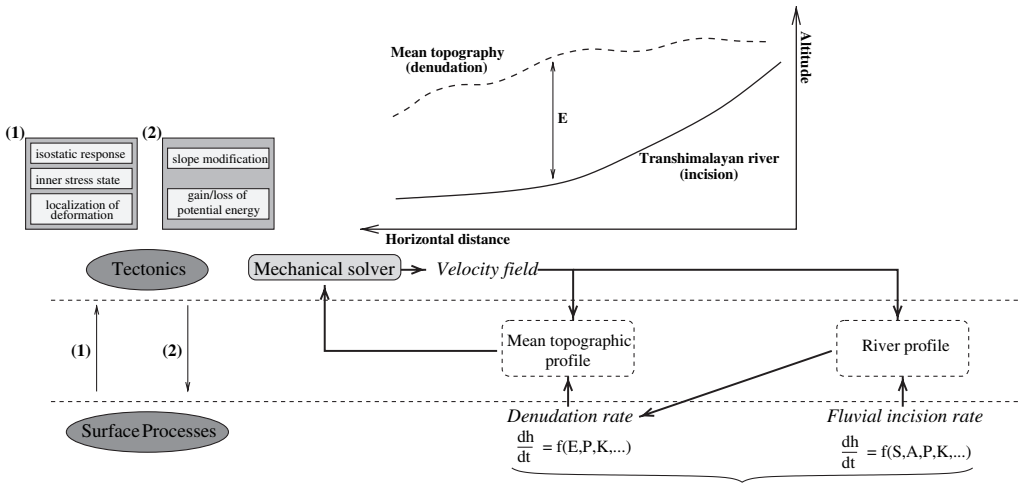

Fig. 6. Relationship between the mechanical solver and the surface processes computation. S: slope of the river, A: area of the watershed, P: precipitation over the watershed, K: erodability, E: entrenchment.

a detachment-limited system, the required hydraulic energy to incise bedrock is considered to be much higher than the energy required to transport the eroded sediments toward the foreland basin. In the above formalism, the sediments are systematically and efficiently evacuated from the range and do not play any explicit role in erosion processes, so mass conservation is not strictly required.

Controlling parameters in fluvial incision and landscape denudation

The threshold τ_c of the incision law is close to the threshold of pebble motion in rivers and, in steep mountains, much lower than average shear stress. Neglecting this threshold term in Equations 9 and 11 provides two simple expressions for river incision and landscape denudation, as the products of a local stream or regional topographic gradient (Δh and S respectively) and of a coefficient which depends on several factors. The denudation term depends on local precipitation, local erodability and valley width L (embedded in k_2). The main trans-Himalayan river incision depends not only on local erodability and valley width, but also on regional precipitation as averaged over the length of its contributing area. For a mountain range subjected to uniform erodability conditions and precipitation, the study of coupling between erosion and tectonics can be reduced to an investigation of the role of a single erosion parameter, $E^* = f(P, K)$. Depending on the precipitation exponent γ, the sensitivity of the system to precipitation can be viewed as weak relative to the sensitivity to abrasion rock strength. For a precipitation exponent $\gamma = 0.33$ and according to Equations 9 and 11, increasing the precipitation by a factor 8 is equivalent to increasing the erodability by a factor 2.

However, the Himalayas display large cross-range variations in precipitation and rock types. Because of these variations, and because tributary denudation and main river incision depend on local and integrated precipitation respectively, the above non-dimensional analysis and reliance on a single erosive parameter loose their validity. To investigate these complexities in the interaction between landscape denudation, main river incision and tectonics, we consider different case studies in which the erodability and precipitation profiles are varied independently. To illustrate lateral (Fig. 1) and cross-range variations in precipitation, a series of profiles representing the lateral amplitude variation of rainfalls in Nepal will first be tested.

Rock types across the Himalayan range display strong variation, from poorly cemented sandstones in the Siwalik Hills, to schists, quartzite and sandstones in the LH, or gneissic units in the HH, or sedimentary units in the South Tibetan series (Fig. 7). A recent study (Attal & Lavé 2006) has shown that these lithologic variations can lead to differences up to 3 orders of magnitude in pebble abrasion rates. Similarly, the bedrock erodability of the Siwalik units represents an erodability coefficient 15 times larger than the LH units: $K_{\mathrm{siw}} = 1.05 \times 10^{-1}$ mm yr^{-1} Pa^{-1} and $K_{\mathrm{LH}} = 0.76 \times 10^{-2}$ mm yr^{-1} Pa^{-1}, respectively

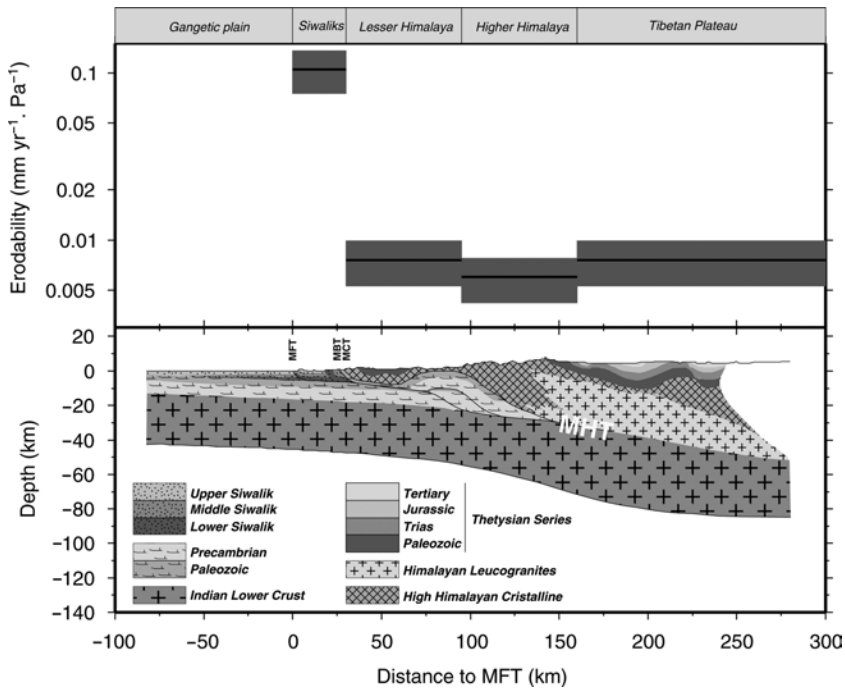

Fig. 7. Erodability values determinated across Central Nepal (Lavé & Avouac 2001) and corresponding geological cross-section modified from Lavé & Avouac (2001). MBT: Main Boundary Thrust; MCT: Main Central Thrust.

(Lavé & Avouac 2001). In order to evaluate the sensitivity of our model to this parameter, we test different kinds of profiles. First we consider that erodability in the Siwalik Hills is K_{siw} while the erodability of the Lesser Himalaya (K_{LH}) is applied to the entire range north of the frontal foothills. Then, we consider homogeneous profiles across the range, where no variation of erodability is considered, with erodability ranging from $0.5 \times 10^{-2}\,\mathrm{mm\,yr^{-1}\,Pa^{-1}}$ to $2 \times 10^{-2}\,\mathrm{mm\,yr^{-1}\,Pa^{-1}}$. Finally, considering that the erodability in the HH has been evaluated by Lavé and Avouac (2001) such that K_{HH} *c.* 0.8 K_{LH}, we introduce this variation to evaluate the influence of slight changes in erodability.

Reference model

From the observations of Figures 2 and 7, two reference profiles are defined for both precipitation and erodability. These two profiles are used as an input for the modelling. The results obtained with this model (Fig. 8, hereafter refered to as the reference model) are in good agreement with the available data sets in the study area (Fig. 1).

The horizontal velocity profile (relative to India) shows that the $20\,\mathrm{mm\,yr^{-1}}$ of convergence applied as a boundary condition are transferred to the MFT. This is related to the low-friction coefficient of the fault, which allows free slip on it. The calculated convergence rate across the range is in agreement with the data, including (1) the horizontal shortening deduced from the uplift of fluvial terraces in the Siwalik foothills (Lavé & Avouac 2001), (2) the progradation of the Gangetic Plain sediments associated with the flexure of the Indian plate (Lyon-Caen & Molnar 1985), and (3) South Tibet Quaternary grabens extension (Armijo *et al.* 1986). Due to gravitational collapse of the range, the horizontal velocity is slightly higher than $20\,\mathrm{mm\,yr^{-1}}$ in the Lesser Himalaya.

This gravitational collapse also accounts for the offset of the calculated topographic profile, which is shifted southward relative to the present-day topography. However, it still preserves both the clear slope transition between the HH and the LH, and the respective average values of slopes in those areas. The present-day topography is used as initial profile for both the mean topography and the main trans-Himalayan river. To allow a significant entrenchment to be created before the beginning of the effective simulation period, the incision of the main

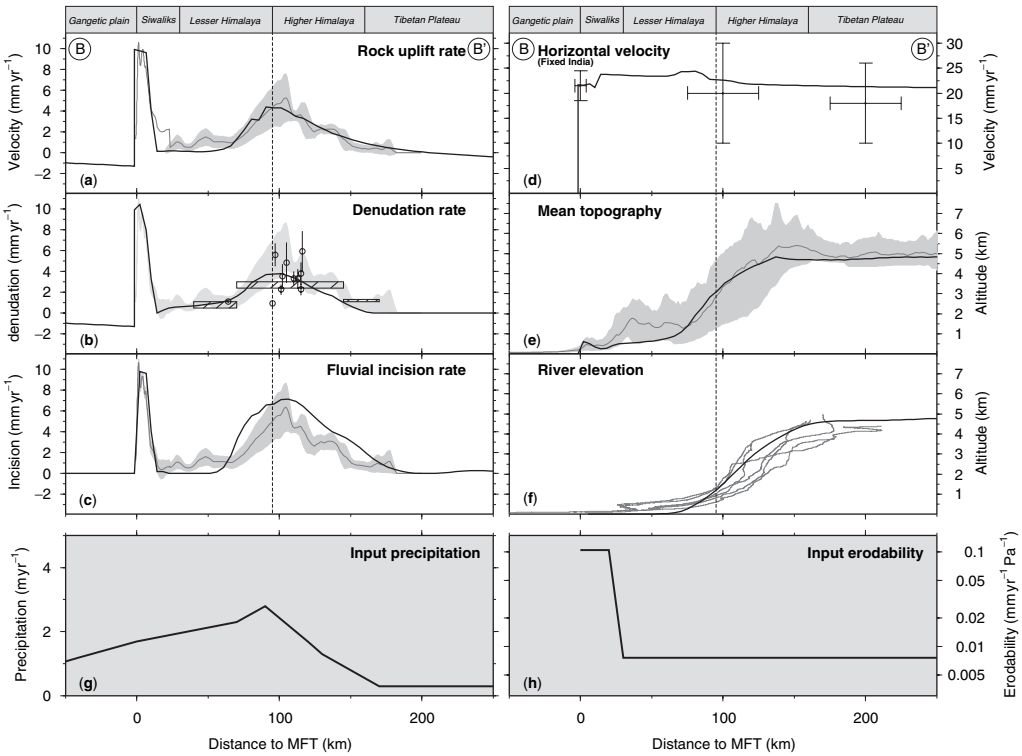

Fig. 8. Reference model. Thick black lines represents model outputs averaged on the last 1% of computation time. The data used to constrain the model outputs are listed below, see text for details. (**a**) Uplift profile, data from Lavé and Avouac (2001): mean value (solid thin line) and 1σ confidence interval (grey area). (**b**) Denudation profile, fission track data from Burbank *et al.* (2003) and averaged cosmogenic denudation rates from Vance *et al.* (2003) (dashed boxes). (**c**) Fluvial incision profile, data from Lavé & Avouac (2001): mean value (solid thin line) and 1σ confidence interval (grey area). (**d**) Horizontal velocity profile, control points from Lavé and Avouac (2000), Lyon-Caen & Molnar (1985) and Armijo *et al.* (1986) (north to south). (**e**) Topographic profile, data derived from GTOPO30 DEM mean (solid thin line) and extreme values (grey area). (**f**) River profile, trans-Himalayan river profiles from Lavé and Avouac (2001). (**g**) and (**h**) present rainfall and erodability profiles used as an input in the modelling. Note that time parameterization is different than that used by Godard *et al.* (2004).

trans-Himalayan river starts at the beginning of the simulation, while the denudation of topography begins later (Fig. 4). Even though the river profile does not reach a strict steady state, it tends to stabilize at the end of the run (Fig. 9). The modelled river profile displays a shape which is in the range of that observed for the main rivers crossing the range.

Fluvial incision rates across the range were calculated by Lavé and Avouac (2001) from a detachment-limited fluvial incision law calibrated in the Siwaliks and the LH. The incision rates on the main trans-Himalayan river computed from Equation 10 give values slightly higher than the data. However, the wavelength and position of the extrema in the Siwaliks and at the LH-HH boundary are consistent with observations.

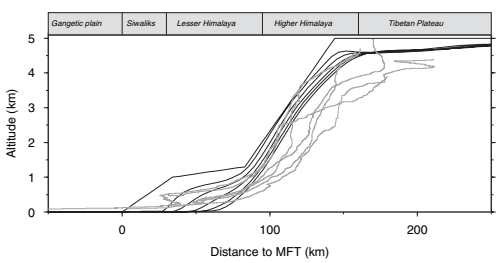

Fig. 9. Evolution of the river profile during the reference run (black lines). The time interval between each profile is *c.* 60 ka. The grey lines represent observed trans-Himalayan river profiles.

Denudation is compared with exhumation rates deduced from apatite fission-track ages in the HH (Burbank *et al.* 2003) and cosmogenic dating of river sediments, which provide an estimation of short-term denudation rate on the watershed (Vance *et al.* 2002). An estimation of uplift rates across the range was deduced from the fluvial incision profile (Lavé & Avouac 2001). This data set indicates that denudation and uplift reach a maximum in the Siwaliks and at the boundary between the Lesser and Higher Himalaya and decrease to a minimum in the LH and South Tibet. Computed denudation and vertical velocity profiles from the model display similar patterns, which are consistent in amplitude and wavelength with what is observed in Central Nepal.

A maximum for uplift, denudation and incision can be observed in the Siwaliks; its presence is mainly due to the high erodability value assigned to this area. The localization of another maximum at the LH-HH boundary can be associated with three mechanisms: (1) presence of a high precipitation zone in the HH, (2) localization of high river slopes in this area, implying high incision rates and, as a result, high entrenchment and denudation, and (3) existence of a ramp for the MHT below the HH. The relative importance of those three contributions is examined in the two next sections.

Sensitivity to precipitation patterns

Influence of rainfall amplitude

The precipitation (collected by the hydrographic network) directly influences the incision on the main trans-Himalayan river according to Equations 10 and 11. The response of the system was tested for various rainfall profiles (Fig. 10), which differ in the amplitude of precipitation in the high range. The erodability profile is the same as for the reference model (Fig. 8).

The increase of precipitation at the LH-HH transition leads to higher denudation rates in this area, whereas the changes in rainfall have no significant effects on denudation in the southern part of the LH. This can be related to the fact that the rock-uplift is close to 0 in the LH, which reduces the sensitivity of the river to the variations of discharge. Fluvial incision of the trans-Himalayan rivers is much less affected than the local incision along tributaries (inferred from the denudation profile) and is, therefore, less than the topographic denudation. This is because discharge along the trans-Himalayan rivers reflects the integration of precipitation along the whole profile and because precipitation is kept constant in South Tibet. Furthermore the variability of incision in the HH leads to important variations of entrenchment (i.e., difference of elevation between the topographic and river profiles, Δh_{total} in Eqn 12), which propagates to the denudation rates in this area.

The near steady-state topographic profile is relatively insensitive to variations in precipitation at the timescale of our study. The increase in denudation near the LH-HH boundary is thus correlated to an increase in the uplift in this area. This highlights a level of coupling between tectonics and erosion, where increased precipitation induces more denudation and more uplift as an isostatic response. As a counterbalance, the uplift, by increasing topographic gradients and tributary relief, will favour an increase in landscape denudation.

Constant precipitation rates over the range

In order to quantify the effects of the rainfall distribution, the behaviour of the model is tested for a set of profiles where precipitation rates are constant between the MFT and southern Tibet. This constant precipitation rate ranges from 0.3 m yr^{-1} to 3.5 m yr^{-1}. On the Tibetan Plateau the precipitation rate falls to 0.3 m yr^{-1} for all the profiles (Fig. 11), to take into account the orographic barrier of the HH. The results reveal that the model is relatively insensitive to the existence of a maximum in precipitation at the LH-HH transition.

When comparing simulations with constant rainfall over the range to what is obtained with the reference model, it appears that the existence of a high precipitation zone between the HH and the LH does not have a noticeable consequence, in our model, on the position of the maximum for denudation, incision or uplift. However the amplitude of this maximum depends directly on the amount of precipitation provided to the system.

The uplift pattern stays unchanged whatever the rainfall profiles, with a maximum at the transition between the HH and the LH. Part of this is due to the rather low value of the precipitation exponent ($\gamma = 0.33$) in the detachment limited incision law (Eqns 10 and 11). In area/slope analysis (Whipple & Tucker 2002), the discharge/area or precipitation exponents cannot be measured, but only estimated relative to the slope exponent. Some studies along rivers draining regions with variable uplift rates (Tomkin *et al.* 2003; Van der Beek & Bishop 2003) have, however, proposed absolute values for the discharge/area exponent, but with large uncertainties. According to Lavé & Avouac's study (2001) in the Siwaliks, and based also on

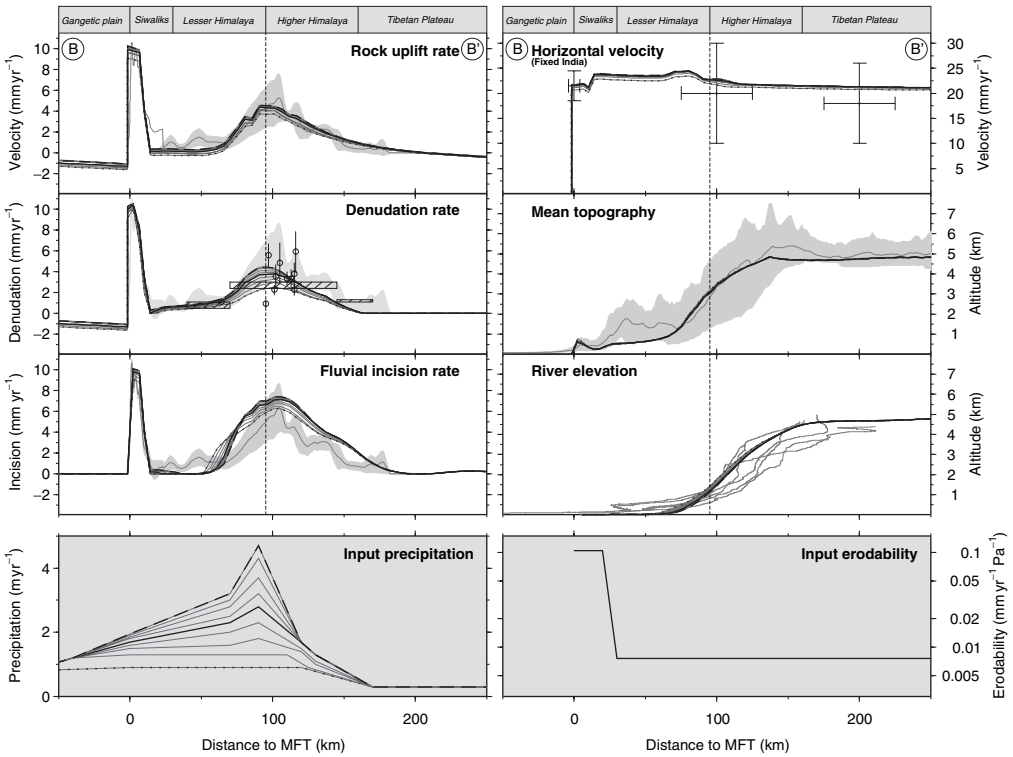

Fig. 10. Results of the simulations with various rainfall profiles. Dashed and dotted lines refer to the maximum and minimum rainfall profiles respectively. The solid bold line is the reference model presented in Fig. 8. The data sets used to compare with the model outputs are the same as in Fig. 8.

a larger data set of worldwide rivers, Lavé and Attal (2003) suggest that the shear stress exponent in the detachment limited incision law is ranging between 0.7 and 1.3. Consequently, the precipitation exponent would range between 0.23 and 0.43. Even though more work is still required to better assess the physical expression of bedrock incision laws, we hypothesize that the sensitivity of incision to precipitation is relatively low. In contrast with previous studies (Thiede *et al.* 2004), it brings the idea that the maximum for rock uplift at $x \sim 100$ km, observed both in the model outputs and the data from Lavé and Avouac (2001), is mainly related, in our model, to the ramp-flat geometry of the MHT rather than to the location of the peak of precipitation.

Sensitivity to erodability

Constant erodability

A set of profiles with constant erodability from the MFT to the Tibetan Plateau, ranging from 2.5×10^{-3} mm yr^{-1} Pa^{-1} to 2×10^{-2} mm yr^{-1} Pa^{-1} were tested (Fig. 12). Due to the linear relationship between erodability and both incision and denudation rates (Eqns 10 and 11), a slight increase in erodability has important implications on the global behaviour of the model.

Increasing erodability leads to higher incision and denudation rates and a coincident augmentation in the uplift rate. The sensitivity is maximum in the HH, where the use of an erodability of 2×10^{-2} mm yr^{-1} Pa^{-1} leads to denudation rates up to 10 mm yr^{-1} in the HH, which far exceed the values of the denudation rate estimated in this area. Erodabilities in the $0.5–1 \times 10^{-2}$ mm yr^{-1} Pa^{-1} range gives values for denudation and uplift in much better agreement with the observations.

Variations of erodability strongly influence both the amplitude and the location of the maximum of fluvial incision rate. This can be related to the regressive incision of the main trans-Himalayan river in response to increasing erodability, which offsets both the maximum for

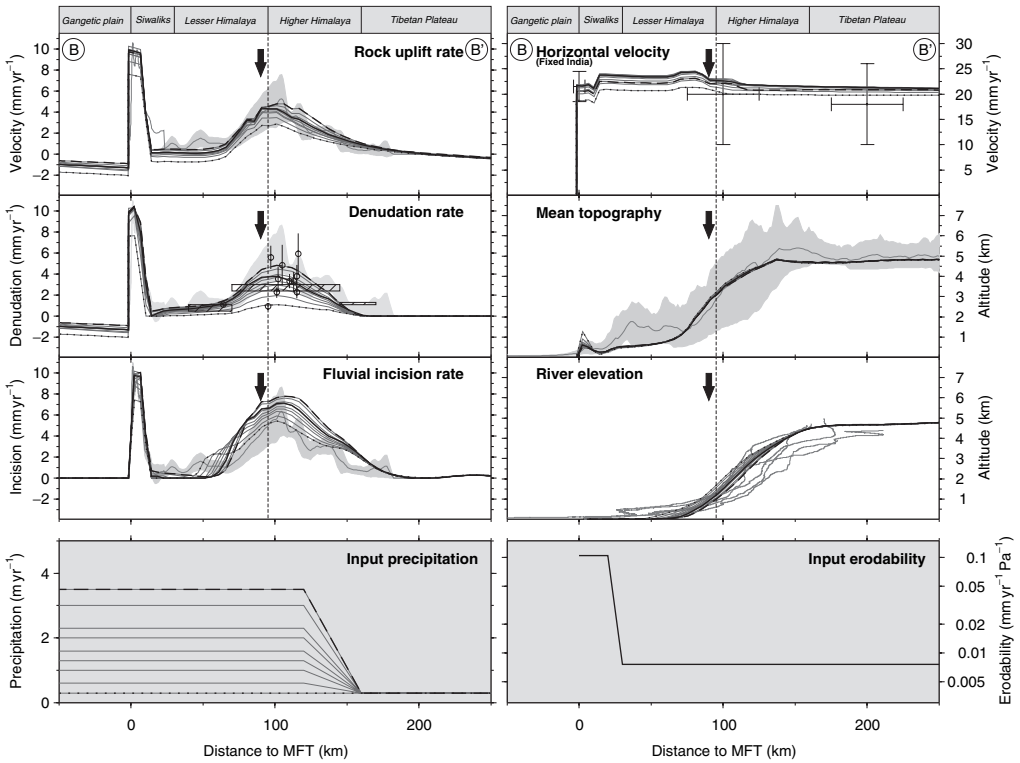

Fig. 11. Results of simulations where the precipitation rate is assumed to be constant from the MFT to southern Tibet, ranging from 0.3 m yr^{-1} to 3.5 m yr^{-1}. Dashed and dotted lines refer to the maximum and minimum rainfall profiles, respectively. The solid bold line is the reference model presented in Fig. 8. The black arrow indicates the maximum of the reference rainfall profile (Fig. 8). The data sets used to compare with the model outputs are the same as in Fig. 8.

the slope of the river and the maximum in incision northward, in accordance with Equation 10. The topographic profile exhibits a lower sensitivity to erodability than does the river profile. More surprisingly, horizontal velocities are significantly affected by the variations of erodability. The rate of convergence in the frontal foothills, like the uplift rates, decreases with increasing rock strength (i.e., with erodability decrease). This phenomenon appears to reflect the role of erosion in stripping crustal material and in favouring the full transfer of the convergence toward the frontal structures.

Changes of erodability along the transect

The models presented in the previous section assume relatively low erodabilities in the Siwaliks foothills, in comparison with the value calculated by Lavé and Avouac (2001) of 1.05×10^{-1} mm yr^{-1} Pa^{-1}. This leads to the development of an unrealistic *c.* 2000 m-high topographic front that cannot be counterbalanced by erosion (the run duration does not permit the equilibrium topography to be reached so this value represents a minimum value). The introduction of a high erodability zone in the Siwalik associated with the unconsolidated sandstones of the foothills, is thus required, first, to obtain a reasonable topographic front in this area, and second, to be able to localize deformation and a very high uplift rate without propagating the deformation southward.

Finally, a more refined erodability profile (dash-dot line, Fig. 12), which imposes slightly lower erodability at the LH-HH boundary in comparison with the southern LH (6×10^{-3} mm yr^{-1} Pa^{-1} instead of 7.6×10^{-3} mm yr^{-1} Pa^{-1} in the reference model), is tested. This low variation of erodability does not have noticeable effects on horizontal shortening and topography. However, the calculated river profile is significantly less entrenched than in the reference case, and it induces a decrease of 1–2 mm yr^{-1} for incision, denudation and uplift rates in the HH. One noteworthy point is

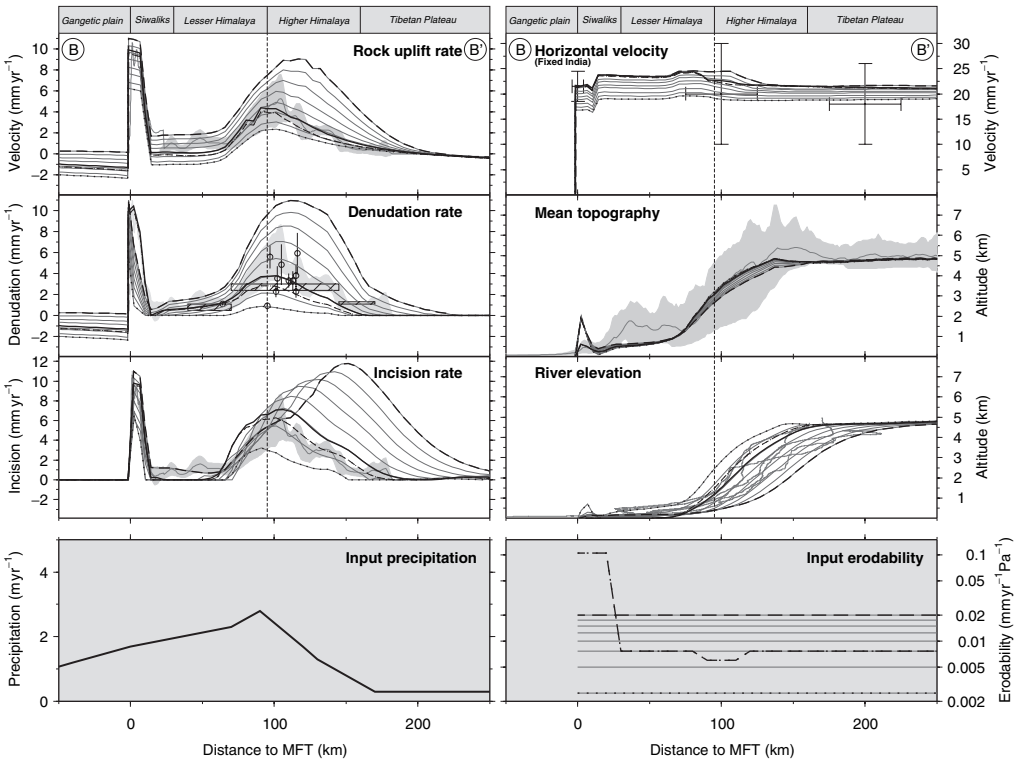

Fig. 12. Results of the simulations for various erodability profiles. Dashed and dotted lines refer to the maximum and minimum erodability profiles, respectively. The solid thick line is the reference model presented in Fig. 8. Dot dashed black line represents the case where a distinction of erodability is made between the different units of the range. The data sets used to compare with the model outputs are the same as in Fig. 8.

that the area affected by this modification (in comparison to the reference profiles) is wider and extends farther north than the defined low erodability area (*c.* 60 km against *c.* 30 km). This is interpreted as a response to an upstream adjustment of the main river near-equilibrium profile, which tends to be less steep. It leads to less entrenchment and, as a consequence, to a relative diminution of denudation and rock-uplift in an area wider than just the low erodability zone.

Discussion and conclusions

Godard *et al.* (2004) have shown that the choice of the erosion law in the modelling of an orogenic system can strongly influence the results of the models and the associated interpretations. Using a fluvial incision formulation, instead of, for example, a classical diffusion law, brings some significant improvements. In particular, an incision-driven model allows the use of external parameters in modelling, measurable on the field, such as precipitation and erodability. The goal of this study was to test the behaviour of the system in response to variations of those two quantities in terms of both amplitude and spatial distribution.

Erodability is a relatively poorly constrained parameter, and even if its importance in orogenic evolution has been recognized (Schlunegger & Simpson 2002) in most modelling, it is considered as uniform. The results presented in this study clearly reveal that rock strength has a first-order control on the evolution of an orogenic wedge and that lithologic considerations really matter when introducing a denudation formulation in a mechanical model. Furthermore, this study demonstrates the predominant role of the high erodability of the Siwalik sediment in the localization of the deformation front and in the regulation of topography.

Moreover, it appears that small variations in erodability (for example between the HH and the LH), may have small, but significant, consequences on the amplitude of denudation and

uplift. As significant uncertainties are often associated with the quantification of the erodability coefficient, it appears that systematic study of the relationship between lithology and erodability is required to develop realistic coupled modelling of tectonics and surface processes. This perspective is certainly influenced by the way denudation processes are formulated in this study and is perhaps particularly relevant to our area of interest. Nevertheless the erodability parameter may still have a predominant control on the modalities of landscape denudation, as observed with the almost linear relationship existing between this parameter and the total sediment flux (Fig. 13).

Due to the values of the parameters used in the fluvial incision formulation, our modelling is less sensitive to rainfall than to erodability (exponent $\gamma = 0.33$ for precipitation, linear dependency for erodability). Precipitation is far better documented than erodability, but the spatial and temporal variabilities of both parameters are extremely important. The approach used in this study was to consider only first-order long-wavelength features characterizing the spatial distribution of precipitation, as, for example, the rain shadow between the HH and Tibetan Plateau (Fig. 2). The amplitude of precipitation directly controls the amplitude of denudation and uplift (Figs 10 and 11). However, the spatial distribution of rainfall seems to have a limited impact on the behaviour of the system, given that the presence or absence of a localized high-precipitation area at the LH-HH boundary does not induce noticeable modifications of the uplift pattern in this area, although it clearly affects the magnitude of denudation. The important variable to take into account is the global volume of water provided to the system by precipitation (Fig. 14). The relative distribution of that precipitation in the range has second order effects and does not modify the global amount of sediment eroded from the system (Fig. 14). Short-wavelength variations exist (Fig. 1) but the results presented in this study show that their relative influence on the tectonics of the system is limited. Our study demonstrates that the existence of localized high denudation and uplift rates can be related to lithology (high erodability in the Siwaliks) or structural and morphological features (ramp-flat geometry of the MHT, high slopes in the HH), rather than to a particular high precipitation area, as suggested by Thiede *et al.* (2004). In a mechanically coupled system, the tectonic behaviour is mostly sensitive to the global amount of precipitation and not to small-scale variations: in the case of the Himalayas, looking for spatial correlation between denudation and precipitation at a wavelength smaller than 20–40 km is not likely to be justified.

Such phenomena and the general low sensitivity of the chosen fluvial incision law to precipitation could explain the recent data along the Marsyandi river in Central Nepal (Burbank *et al.* 2003). This study displays a zone across the HH with uniform values of the FT closure

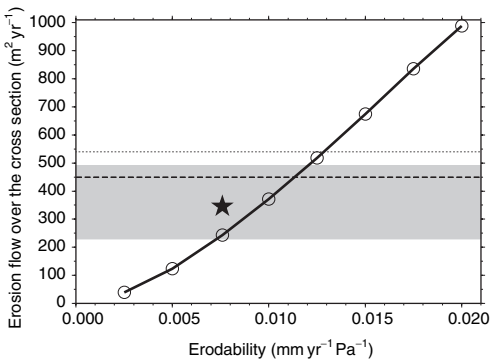

Fig. 13. Erodability versus outcoming flux of sediments for the constant erodability simulations (Fig. 12). The grey area, the dashed and dotted bold lines represent the erosion flux estimated by Métivier *et al.* (1999), Pinet and Souriau (1988) and Summerfield and Hutton (1994), respectively. The position of the reference model (Fig. 8) is indicated by the black star. The mean erodability associated with the reference model takes into account the variations of this parameter along the studied profile.

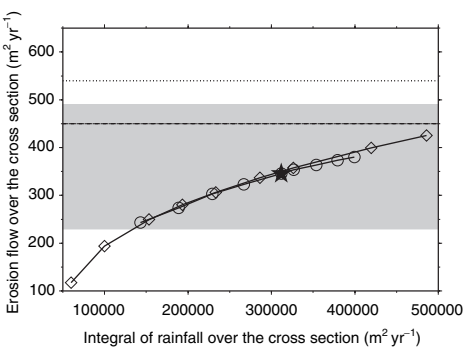

Fig. 14. Integrated precipitations over the cross-section versus outcoming flux of sediments (integration of the denudation profile). Circles and diamonds represent outputs for runs from Figs 10 and 11, respectively (variable precipitation and constant erodability). The black star indicates the position of the reference model (Fig. 8). The data are the same as in Fig. 13.

ages in apatite, and probably of the denudation rates, despite a three to four fold drop of the rainfall profile across the HH. These ages would primarily reflect the underlying uniform tectonic uplift associated with the mid-crustal ramp, and the lower sensitivity of the trans-Himalayan rivers to the local precipitation. This illustrates the difficulties or, perhaps, the systematic bias in trying to correlate local rainfall with local denudation to demonstrate or invalidate coupling between tectonics and climate.

Our assumption that applied present-day observed rainfall amplitudes to the timescale of the Quaternary in our simulations could be questioned. In particular, the influence of short to middle term evolution of climatic variables (e.g., monsoon, glaciations) on the tectonics of mountain ranges is still unclear and is worth investigating.

Most of the illustrations of this paper were prepared using GMT (Wessel & Smith 1991). We are grateful to J. Chéry and R. Hassani for providing the finite element code and Y. Dramais for corrections on the manuscript. Constructive reviews by F. Schlunegger, D. W. Burbank and one anonymous reviewer contributed to improve the manuscript. This work is supported by a RELIEF grant from the Centre National de la Recherche Scientifique.

References

ARMIJO, R., TAPPONIER, P., MERCIER, J. L. & TONGLIN, H. 1986. Quaternary extension in southern Tibet. *Journal of Geophysical Research*, **91**, 13803–13872.

ATTAL, M. & LAVÉ, J. 2006. Changes of bedload characteristics along the Marsyandi River (central Nepal): Implications for understanding hillslope sediment supply, sediment load evolution along fluvial networks and denudation in active orogenic belts. *In*: WILLETT, S. D., HOVIUS, N., BRANDON, M. T. & FISHER, D. (eds), *Tectonics Climate, and Landscape Evolution*, Geological Society of America Special Paper, **398**, p. 143–171, DOI: 10.1130/2006.2398(09).

AVOUAC, J. P. & BUROV, E. B. 1996. Erosion as a driving mechanism of intracontinental mountain growth. *Journal of Geophysical Research*, **101**, 17747–17769.

BEAUMONT, C., JAMIESON, R. A., NGUYEN, M. H. & LEE, B. 2001. Himalayan tectonics explained by extrusion of a low-viscosity crustal channel coupled to focused surface denudation. *Nature*, **414**, 738–742.

BILHAM, R. K., LARSON, K., FREYMULLER, J. & PROJECT IDYLHIM MEMBERS, 1997. Indo-Asian convergence rates in the Nepal Himalayas. *Nature*, **386**, 61–64.

BURBANK, D. W., LELAND, J., FIELDING, E., ANDERSON, R. S., BROZOVIC, N., REID, M. R. & DUNCAN, C. 1996. Bedrock incision, rock uplift and threshold hillslopes in the northwestern Himalayas. *Nature*, **379**, 505–510.

BURBANK, D. W., BLYTHE, A. E. *ET AL.* 2003. Decoupling of erosion and precipitation in the Himalayas. *Nature*, **426**, 652–655.

CARTER, N. L. & TSENN, M. C. 1987. Flow properties of continental lithosphere. *Tectonophysics*, **136**, 27–63.

CATTIN, R. & AVOUAC, J. P. 2000. Modelling moutain building and the seismic cycle in the Himalaya of Nepal. *Journal of Geophysical Research*, **105**, 13389–13407.

CATTIN, R., MARTELET, G., HENRY, P., AVOUAC, J. P., DIAMENT, M. & SHAKYA, T. R. 2001. Gravity anomalies, crustal structure and thermo-mechanical support of the Himalayas of Central Nepal. *Geophysical Journal International*, **147**, 381–392.

CHEN, Q., FREYMUELLER, J. T., YANG, Z., XU, C., JIAN, W., WANG, Q. & LIU, J. 2004. Spatially variable extension in southern Tibet based on GPS measurements. *Journal of Geophysical Research*, **109**, DOI 10.1029/2002JB002350.

GAME DATA CENTRE. 2005. World Wide Web address: ftp://ftpprd.ncep.noaa.gov/pub/cpc/fews/S.Asia/

GODARD, V., CATTIN, R. & LAVÉ, J. 2004. Numerical modelling of mountain building: interplay between erosion law and crustal rheology. *Geophysical Research Letters*, **31**, DOI 10.1029/2004GL021006.

HASSANI, R., JONGMANS, D. & CHÉRY, J. 1997. Study of plate deformation and stress in subduction processes using two-dimensional numerical models. *Journal of Geophysical Research*, **102**, 17951–17965.

HENRY, P., LE PICHON, X. & GOFFÉ, B. 1997. Kinematic, thermal and petrological model of the Himalayas: constraints related to metamorphism within the underthrust Indian crust and topographic elevation. *Tectonophysics*, **273**, 31–56.

HOVIUS, N., STARK, C. P. & ALLEN, P. A. 1997. Sediment flux from a mountain belt derived from landslide mapping. *Geology*, **25**, 231–234.

HOWARD, A. D., DIETRICH, W. E. & SEIDL, M. A. 1994. Modelling fluvial erosion on regional to continental scales. *Journal of Geophysical Research*, **99**, 13971–13986.

INDIAN INSTITUTE OF TROPICAL METEOROLOGY (IITM). 2005. World Wide Web address: http://www.tropmet.res.in/

KIRBY, S. H. & KRONENBERG, A. K. 1987. Rheology of the lithosphere: Selected topics. *Reviews of Geophysics*, **25**, 1219–1244.

LARSON, K. M., BURGMANN, R., BILHAM, R. & FREYMULLER, J. 1999. Kinematics of the India-Eurasia collision zone from GPS measurements. *Journal of Geophysical Research*, **104**, 1077–1094, DOI 10.1029/1998JB900043.

LAVÉ, J. 2005. Analytic solution of the mean elevation of a watershed dominated by fluvial incision and hillslopes landslides. *Geophysical Research Letters*, **32**, L11403, DOI 10.1029/2005GL022482.

LAVÉ, J. & ATTAL, M. 2003. Landscape evolution due to river incision in active mountains. *Geophysical Research Abstracts*, **5**.

LAVÉ, J. & AVOUAC, J. P. 2000. Active folding of fluvial terraces across the Siwaliks Hills, Himalayas of central Nepal. *Journal of Geophysical Research*, **105**, 5735–5770.

LAVÉ, J. & AVOUAC, J. P. 2001. Fluvial incision and tectonic uplift across the Himalayas of central Nepal. *Journal of Geophysical Research*, **106**, 26561–26591.

LE FORT, P. 1986. Metamorphism and magmatism during the Himalayan collision. *In*: COWARD, M. P. & RIES, A. C. (eds) *Collision Tectonics*. Geological Society Special Publications, **19**, 159–172.

LYON-CAEN, H. & MOLNAR, P. 1985. Gravity anomalies, flexure of the Indian plate, and the structure support and evolution of the Himalaya and Ganga basin. *Tectonics*, **4**, 513–538.

MÉTIVIER, F., GAUDEMER, Y., TAPPONIER, P. & KLEIN, M. 1999. Mass accumulation rates in Asia during the Cenozoic. *Geophysical Journal International*, **137**, 280–318.

MOLNAR, P. 2003. Nature, nurture and landscape. *Nature*, **426**, 612–614.

NEPALESE METEOROLOGICAL FORECASTING DIVISON (NMFD). 2005. World Wide Web address: http://www.mfd.gov.np.table.php

NOAA CLIMATE PREDICTION CENTRE. 2005. World Wide Web address: http://hydro//iis.u-tokyo.ac.jp/GAME-T.GAIN-T/routine/Nepal

PANDEY, M. R., TANDUKAR, R. P., AVOUAC, J. P., LAVÉ, J. & MASSOT, J. P. 1995. Interseismic strain accumulation on the Himalayan crustal ramp (Nepal). *Geophysical Research Letters*, **22**, 751–754.

PINET, P. & SOURIAU, M. 1988. Continental erosion and large scale relief. *Tectonics*, **7**, 563–582.

SCHELLING, D. & ARITA, K. 1991. Thrust tectonics, crustal shortening and the structure of the Far Eastern Nepal Himalaya. *Tectonics*, **10**, 851–862.

SCHLUNEGGER, F. & SIMPSON, G. 2002. Possible erosional control on lateral growth of the European Central Alps. *Geology*, **30**, 907–910.

SUMMERFIELD, M. A. & HUTTON, N. J. 1994. Natural control of fluvial denudation rates in major world drainage basins. *Journal of Geophysical Research*, **99**, 13871–13883.

THIEDE, R. C., BOOKHAGEN, B., ARROWSMITH, J. R., SOBEL, E. R. & STRECKER, M. R. 2004. Climatic control on rapid exhumation along the Southern Himalayan Front. *Earth and Planetary Science Letters*, **222**, 791–806.

TOMKIN, J. H., BRANDON, M. T., PAZZAGLIA, F. J., BARBOUR, J. R. & WILLETT, S. D. 2003. Quantitative testing of bedrock incision models for the Clearwater River, NW Washington State. *Journal of Geophysical Research*, **108**, 2308, DOI 10.1029/2001JB000862.

TSENN, M. C. & CARTER, N. L. 1987. Upper limits of power law creep of rocks. *Tectonophysics*, **136**, 1–26.

UNDERWOOD, P. 1983. *Dynamic Relaxation. Computational Methods for Transient Analysis*. Elsevier, Amsterdam, 245–265.

VANCE, D., BICKLE, M., IVY-OCHS, S. & KUBIK, P. W. 2003. Erosion and exhumation in the Himalaya from cosmogenic isotope inventories of river sediments. *Earth and Planetary Science Letters*, **206**, 273–288.

VAN DER BEEK, P. A. & BISHOP, P. 2003. Cenozoic river profile development in the Upper Lachlan catchment (SE Australia) as a test of quantitative fluvial incision models. *Journal of Geophysical Research*, **108**, 2309, DOI 10.1029/2002JB002125.

WESSEL, P. & SMITH, W. H. F. 1991. Free software helps map and display data. *EOS Transactions AGU*, **72**, 441, 445–446.

WHIPPLE, K. X. & TUCKER, G. E. 1999. Dynamics of the stream-power river incision model: implications for height limits of mountain ranges, landscape response timescales, and research needs. *Journal of Geophysical Research*, **104**, 17661–17674.

WHIPPLE, K. X. & TUCKER, G. E. 2002. Topographic outcomes predicted by stream erosion models: sensitivity analysis and intermodel comparison. *Journal of Geophysical Research*, **107**, 2179, DOI 10.1029/2001JB000162.

WILLETT, S. D. 1999. Orogeny and orography: The effects of erosion on the structure of mountain belts. *Journal of Geophysical Research*, **104**, 28957–28981.

ZHAO, W., NELSON, K. D. & PROJECT INDEPTH TEAM. 1993. Deep seismic-reflection evidence continental underthrusting beneath southern Tibet. *Nature*, **366**, 557–559.